AIP | Review of Scientific Instruments

Gas filter correlation instrument for the remote sensing of gas leaks

H. S. Lee, H. H. Zwick, and S. M. Till

Citation: Review of Scientific Instruments **56**, 1812 (1985); doi: 10.1063/1.1138100
View online: http://dx.doi.org/10.1063/1.1138100
View Table of Contents: http://scitation.aip.org/content/aip/journal/rsi/56/9?ver=pdfcov
Published by the AIP Publishing

Gas filter correlation instrument for the remote sensing of gas leaks

H. S. Lee[a] and H. H. Zwick

MONITEQ Ltd., 630 Rivermede Road, Concord, Ontario L4K 1B6, Canada

S. M. Till

Canada Centre for Remote Sensing, 2464 Sheffield Road, Ottawa, Ontario K1A OY7, Canada

(Received 27 August 1984; accepted for publication 5 June 1985)

An airborne remote sensor named GASPILS (gas pipeline leak sensor) has been developed and tested to detect leaks from natural gas pipelines by monitoring the amount of methane in the atmosphere above the leak. The sensor is a passive electro-optical system, with two independent channels, operating in a downward-looking profiling mode. It is designed to detect increases in the low levels of methane concentration by sensing the infrared spectral radiance signatures using a nondispersive gas filter correlation technique. This technique involves the use of a gas cell as a matched spectral filter, and it combines a high degree of sensitivity to the target gas with a high degree of specificity.

INTRODUCTION

Natural gas pipelines form an extensive network throughout the country. The development of gas leaks, as a result of pipeline aging and dislocations, for example, leads to serious losses of resources and may result in dangerous and costly incidents. Conventionally, pipeline leaks are detected by hand-carried flame ionization detectors which sample and measure the methane gas concentration in the atmosphere above the pipeline. Such a method of leak detection is labor intensive and costly, and can only be done at a slow rate, perhaps once a year or even less frequently.

A new airborne remote sensor name GASPILS has been designed and developed to complement and probably replace the conventional technique. The sensor is a passive downward-viewing electro-optical device which detects the pipeline leak by monitoring the amount of methane gas in the atmosphere above the pipeline. Low levels of methane concentration are detected by means of their infrared spectral signatures, using a nondispersive gas filter correlation technique.

The GASPILS instrument contains two optical channels, one channel sensitive to methane and the other to a second target gas. Each channel has its own detector and optics, and shares the digital signal processing system. The sensor provides simultaneous measurements of the two target gases, the background radiance signals, and ratios of the gas signals. The signal processor is designed to compensate for the effects of temperature and emissivity variations of the ground. Analog and digital outputs are provided, together with audio and visual alarms activated when the gas signal exceeds a preset value. The sensor is designed to be easily modified to monitor different gases so that it may have applications in other fields of trace gas detection.

In this paper we discuss the design of the GASPILS sensor together with laboratory performance test results.

I. GAS FILTER CORRELATION TECHNIQUE

The gas filter correlation technique (GFC) uses a sample of the gas being monitored to provide an efficient and selective spectral filter, and to isolate the radiation absorbed by or emitted from the target gas. The technique has high sensitivity (a) because the filter can have both a large light gathering capability and a wide spectral bandwidth and (b) because the gas sample has a unique spectral signature that matches that of the target gas. These features, together with the simplicity of optical design, make this an attractive technique. Systems based on this nondispersive gas filter correlation technique have been in use for many years. Luft[1] described an early version of this device, and since then, several workers have used similar systems.[2–7] Although numerous GFC sensors have been used in remote sensing of atmospheric trace gases, there are basically two different configurations; one uses the single common optical channel and the other consists of parallel channels. In the single common channel configuration, the sensor modulates the beam path through the correlation gas cell and vacuum cell, having the rest of the optical elements of the sensor in common. The parallel channel configuration uses fixed gas cells and divides the incoming beam into two separate optical channels which contain separate detectors at the end of each channel.

In the single common channel configuration, the beam passes through exactly the same optical elements with the exception of the gas cells minimizing any spurious signals from the incoming radiance and parameters of the optical elements. However, a fast changing scene radiance will cause substantial problems in this configuration. The parallel channel configuration appears to have fewer problems with the scene radiance change if both of the detectors are kept stable. On the other hand, the difficultly associated with the correlation of scene radiance and optical components is a serious problem.[7] In addition, the zero gas signal balancing (to be discussed in Sec. II B) must be continuously updated in this configuration due to the long-term drift in the detector responsivity. The radiance signal itself is another basic signal to be acquired in most of the applications. Therefore, it is often required to monitor the reference blackbody temperature which is precisely known.

In the GASPILS design we used the common channel configuration with a rotating gas cell chopper wheel. In this

 0034-6748/85/091812-08$01.30

way we comply with the hostile airborne environment in terms of electromagnetic noise and large temperature change anticipated. The fast change in scene radiance is then handled by using high chopping frequency and relatively large FOV. The chopping speed is limited up to 40 Hz due to the mechanical stability of the chopper. The $1/f$ noise may decrease by a factor of 2 at a much higher chopping speed (1000 Hz). A high chopping speed is also desirable in terms of potential interference from a fast scene radiance change in the flight mode. However, the preliminary field data, which will be discussed elsewhere in this paper, shows good rejection of the interference from the change in scene radiance. The zero gas balancing is carried out at a fixed gas cell chopper temperature, which is maintained at the preset value throughout operation by means of the insulation of the chopper wheel and use of a TE cooler/heater device. From this temperature setting one can also calculate the absolute radiance values from the output signal (see Sec. II B).

The principle of operation of a gas filter correlation technique will be described briefly. The main feature is a pair of gas cells. One cell, referred to as the correlation gas cell, contains a judiciously chosen quantity of the target gas to be sensed, while the second cell, the reference cell, contains a spectrally inactive gas. The optical depth of gas in the correlation cell at the selected operating spectral band is optimized to maximize the product of the modulation of the incoming radiation power and the average correlation gas cell transmittance. The incoming radiation spectrum from the target is selectively filtered by being absorbed in the sample cell of the same gas, but is readily transmitted through the reference cell. Thus, the radiance transmitted through the sample cell is largely independent of the presence of the target gas, whereas the radiance transmitted through the reference cell is strongly dependent upon the presence of the target gas. The differences in spectral transmittance between the two cells is thus a sensitive indicator of the amount of target gas signature in the incoming radiation received by the sensor.

The difference signal ΔS is proportional to the total amount of target gas in the column subtended by the sensor field of view and can be expressed as

$$\Delta S = A\Omega \int_{\Delta\nu} \left[\eta_c N_T(\nu) e^{-\tau_c(\nu)} - \eta_r N_T(\nu) e^{-\tau_r(\nu)} \right] d\nu + J_c, \tag{1}$$

where η_c and η_r are the transmittance of the optical components for the correlation and the reference channels, respectively. $A\Omega$ is the etendu, $\tau_c(\nu)$ and $\tau_r(\nu)$ are optical depths of the correlation and reference gases, respectively, and J_c is the term for the emission from the correlation gas in the cell. $N_T(\nu)$ is the total upwelling radiance reaching the sensor input lens. For a simplified model of a uniform monolayer atmosphere, the total upwelling radiance $N_T(\nu)$ as viewed by a nadir-type sensor can be written as

$$N_T(\nu) = \left[\epsilon(\nu) B_e(\nu,\theta_e) e^{-\tau_a(\nu)} + B_a(\nu,\theta_a)(1 - e^{-\tau_a(\nu)}) \right], \tag{2}$$

where $B(\nu,\theta)$ is the blackbody radiance at frequency ν, temperature θ, ϵ is the emissivity of the earth's surface, and $\tau_a(\nu)$ is the optical thickness of the target gas. Subscripts e and a designate the earth and atmosphere, respectively. Note that the solar radiation is not included in this expression for simplicity of discussion.

Substituting Eq. (2) into Eq. (1) yields

$$\Delta S = \eta_c A\Omega \left[\epsilon B_e \int_{\Delta\nu} e^{-\tau_a(\nu)} \left(e^{-\tau_c(\nu)} - \frac{\eta_r}{\eta_c} e^{-\tau_r(\nu)} \right) d\nu + B_a \int_{\Delta\nu} (1 - e^{-\tau_a(\nu)}) \left(e^{-\tau_c(\nu)} - \frac{\eta_r}{\eta_c} e^{-\tau_r(\nu)} \right) d\nu \right] + J_c. \tag{3}$$

Here the spectral dependence of $\epsilon(\nu)$ and $B(\nu)$ is regarded as constant within the range of the spectral window $\Delta\nu$.

The GASPILS measurement requires precise balancing of the signals from the correlation gas and reference gas sectors, so that the sensor ΔS signal is insensitive to source radiance changes in the absence of target gas. When the correct balancing is achieved then

$$\eta_c \int_{\Delta\nu} e^{-\tau_c(\nu)} d\nu = \eta_r \int_{\Delta\nu} e^{-\tau_r(\nu)} d\nu. \tag{4}$$

Substituting Eq. (4) into Eq. (3), one can easily obtain

$$\Delta S = \eta_c A\Omega (\epsilon B_e - B_a) \left(\int_{\Delta\nu} T_a T_c \, d\nu - \frac{1}{\Delta\nu} \int_{\Delta\nu} T_a \, d\nu \int_{\Delta\nu} T_c \, d\nu \right) + J_c. \tag{5}$$

Here the spectral response of the reference channel optics is assumed to be flat within the bandwidth, and the optical transmittance $T(\nu)$ used in Eq. (5) is defined as

$$T(\nu) = e^{-\tau(\nu)}. \tag{6}$$

In practice, condition (4) is reached by adjusting the gains applied to the signals from the correlation gas and reference gas sectors, so that those signals are equal in the absence of target gas.

The term

$$\left(\int_{\Delta\nu} T_a T_c \, d\nu - \frac{1}{\Delta\nu} \int_{\Delta\nu} T_a \, d\nu \int_{\Delta\nu} T_c \, d\nu \right),$$

is referred to as the correlation coefficient ρ. The maximum sensitivity of the GFC instrument is obtained by optimizing the product of η_c and the correlation coefficient. It is apparent from Eq. (6) that the optimum correlation cell optical thickness depends on the detailed structure of the correlation gas spectrum. For the GASPILS sensor and methane target gas, a simple monolayer model calculation was used, with radiation from the source (ground) being transferred through the atmosphere, containing the target gas, and passing through the correlation cell. The model used high resolution spectral information[8] for the methane ν_4 band. Since collision broadening is considered to be the major cause of the line broadening, the individual line shape was described using the Lorentzian line profile as follows:

$$K(\nu) = \frac{S}{\pi} \frac{\alpha}{[(\nu - \nu_0)^2 + \alpha^2]}, \tag{7}$$

where α is the half-width, ν_0 is the line center wavenumber, S is the line strength, and $K(\nu)$ is the absorption coefficient of an isolated line.

The temperature dependence of the line strength was described using the partition function and lower state population as

$$S(T) = S_0\left(\frac{T}{T_0}\right)^{1.5} \exp\left(\frac{1.439E''(T-T_0)}{T_0T}\right), \quad (8)$$

where S_0 is the line strength at temperature T_0. The lower state energy E'' for each rotational level j was calculated as[9]

$$E'' = B_0 j(j+1) - D_0[j(j+1)]^2 \quad (9)$$

with

$$B_0 = 5.2412\ \text{cm}^{-1} \text{ and } D_0 = 1.14\times 10^{-4}\ \text{cm}^{-1}. \quad (10)$$

The half-width corrected for the temperature and pressure variation, neglecting Doppler broadening, was given by

$$\alpha = \alpha_0(P/P_0)\sqrt{T_0/T}, \quad (11)$$

where $\alpha_0 = 0.059\ \text{cm}^{-1}$ at $P_0 = 1$ atm and $T_0 = 296\text{K}$.[10].

In evaluating the total absorption coefficient at a fixed wavenumber, all the lines within $\pm$ 12 cm^{-1} were considered and the contribution from each line was summed. The integration in Eq. (5) was carried out numerically digitally for a given set of temperature and pressure. The difference signal ΔS was then calculated according to Eq. (5). In this calculation the term J_c was ignored since the term remains constant in time due to the stabilized temperature controller design feature.

To find the optimum optical thickness of the correlation cell, a set of correlation coefficients was obtained as a function of the correlation gas cell optical thickness for a given target gas optical thickness. The results are illustrated in Fig. 1. The correlation cell thickness was then chosen to be 0.01 m (with atmospheric gas pressure) and was predicted to give a value equal to 0.86 of the maximum (obtained with 0.1-m cell) correlation. The model calculation was also used to study the temperature dependence of the correlation coefficient and showed a slight deterioration (as expected) in the correlation coefficient as the temperature difference between the target gas and the correlation gas increased. This variation in the correlation coefficient due to a few degree changes in temperature was insignificant compared with system noise.

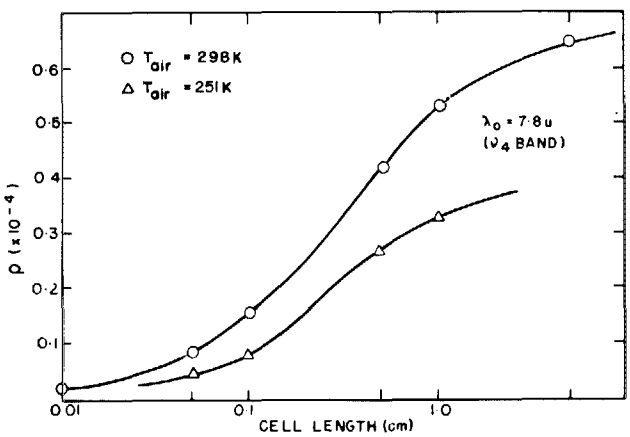

FIG. 1. Correlation coefficients for 10 ppm m CH_4 leak gas as a function of the cell length: $T_g = 300$ K, $T_{cell} = 296$ K.

II. GASPILS DESIGN

The GASPILS sensor uses a signal detector for each channel and passes the incident radiation alternately through the correlation cell and the reference cell. The time sharing configuration has two potential problems when used for high sensitivity detection from a downward-looking moving platform. The first is gas cell temperature instability during the time interval of the modulation which might cause an error signal. The second problem is the change in the scene radiance as the sensor footprint moves across the target. These problems are minimized by temperature control, the optical design chosen, and the use of digital signal interpolation. Also, as in all remote measurements, "false" signals resulting from environmental effects have to be reduced: the measurements should distinguish between leak gas and effects of background methane gas in the atmosphere, atmospheric gases, and solar radiation. To overcome these problems GASPILS employs two channels, one sensitive to methane and the other sensitive to a second target gas such as ethane. The spectral bandpass of the two channels are located at absorption features of the gases, selected at spectral transmission windows of the atmosphere, in the infrared, and where the ground emissivity values for the two bands tend to vary in a similar manner for various ground coverages.

There are two absorption bands available for the methane gas channel in the infrared region and are located at 3.4 and 7.8 μm. The 3.4-μm band overlaps with one of the ethane absorption bands (the other ethane absorption band is located at 12.2 μm). Since the system is limited to dual channels we must select one optimum band for each channel. The selection is based on net gas detection sensitivity and the immunity to the interference. The sensitivity of the sensor using different absorption bands is obtained through the model calculation discussed in the previous section. The model calculation shows tenfold sensivity improvement for the methane detection by using the 7.8-μm band. Therefore, we chose the 7.8-μm band for the methane channel. A similar sensitivity for the ethane detection is predicted for both of the absorption bands.

The function for the second gas channel is twofold: One is to discriminate the possible interference from the time varying parameters, such as the temperature contrast between the ground and the air, the temperature profile in the field of view, and the ground emissivity; and the other is to distinguish the natural gas of biochemical origin and the pipeline leak gas. The first objective may be accomplished by selection of any atmospheric gases mixed uniformly under the assumption that the radiance through that band varies the same way as the radiance through the 7.8-μm band, which means that the emissivity is most likely the same for the various types of ground compositions. According to the existing data,[11] the emissivity at 12.2 μm is very similar to that of the 7.8-μm band for various ground compositions, while the ground emissivity at 3.4 μm is very different from the emissivity at 7.8 μm. The ethane gas is known to be a uniformly mixed trace gas in the atmosphere at a level of 1 ppb.[12] In conclusion, we chose the 7.8-μm band for the

methane channel and the 12.2-μm band for the ethane channel.

The second objective can be met if we use the ethane channel, because the natural gas originating from the bioactivity does not contain ethane gas. The signal processing scheme of GASPILS takes the ratio of the two gas signals to minimize the effects of "hot spots" on the ground, and also to reduce false alarms from background methane which originates from bioactivity at the surface.

A. Optics

A novel optical design, described below in further detail, maximizes the duty factor of the sensor, provides good optical and thermal stability, and provides convenience in optical alignment.

Each of the two optical trains (one for each target gas) is mounted vertically, and contains a collimating lens, gas cells (located in the chopper wheel assembly), field lens, spectral filter, and detector. The lenses are used to seal the chopper wheel housing as shown in Fig. 2.

For a 1-mm^2 detector size, a maximum etendu of 7.4×10^{-2} cm^2 sr was established by a specific fast Ge lens configuration. The optimum field of view of the field lens was then determined based on the nominal sensor platform altitude of 100 m and the optimum footprint size of radius 7 m. The footprint size is selected to be larger than the anticipated plume size since the sensor platform is rather unstable. This way we improve the coverage on the ground which helps to prevent missing the leak spot. The larger footprint also helps to extend the observation duration of the leak so that the loss of the sensitivity by the extended footprint size will be partly recovered at the end. The field lens is mounted on a threaded ring for a few degrees adjustment of the FOV. The collimating lens provides a pseudocollimated beam on the interference filter to minimize the pass-band shift. Finally the detector lens focuses the collimating lens onto the detector to avoid correlation of the ground surface radiance structures with the nonuniform detector sensitivity across the detector area.

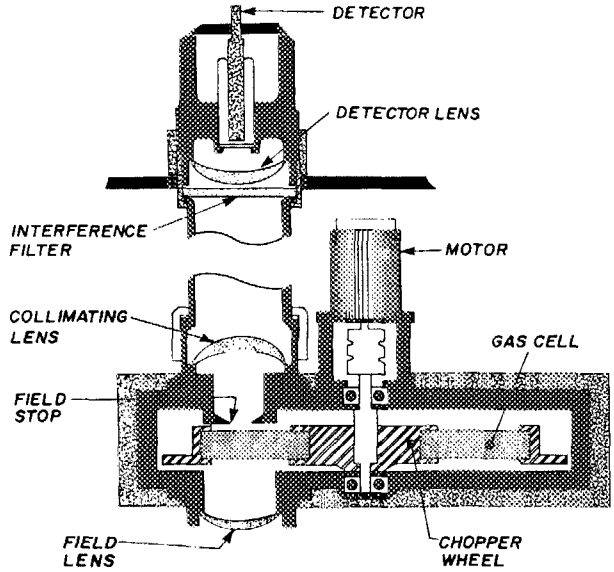

FIG. 2. Schematic of GASPILS optomechanics.

A unique design of the chopper and cell configuration has been used to maximize the duty factor and to simultaneously accommodate the two optical channels. The three gas cells required (two target gas cells and one reference cell) are combined in a single chopper wheel that is used to modulate both channels. By locating the gas cells at different radii on the chopper, the signals for the two target gases are measured simultaneously. An opaque mask covers the cells with slotted sectors to provide windows for the correlation gas cell and reference cell, and a blank sector in appropriate sequences for each channel. Rotation of the disk gives the detector signal outputs shown in the upper half of Fig. 3. The

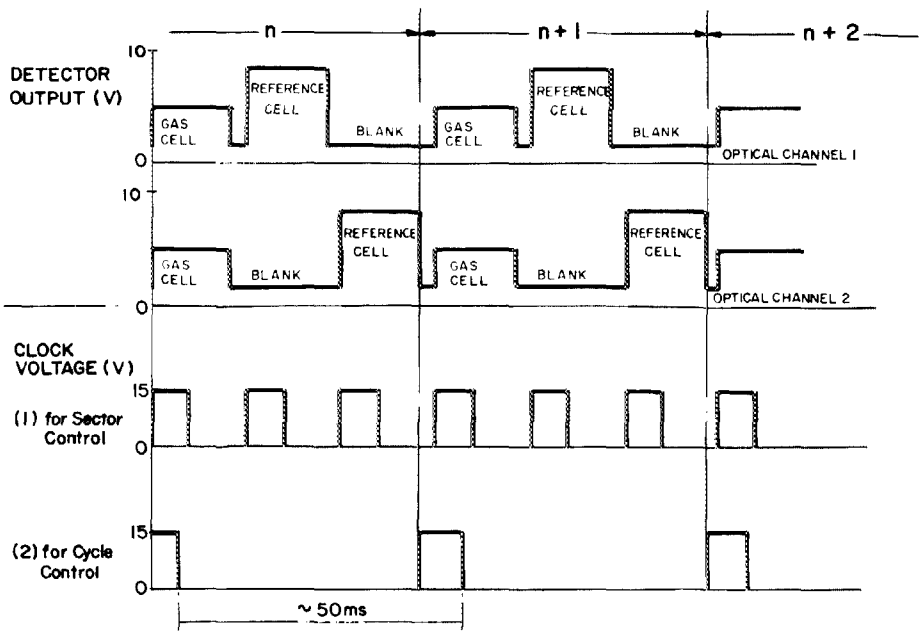

FIG. 3. Schematic of the radiance signal sequences for M and E channels and clock signals.

TABLE I. System parameters.

	CH_4	C_2H_6	Unit
λ	7.91	12.16	μm
$\Delta\lambda$	0.29	0.31	μm
Absorption Coefficient	0.10	0.17	$cm^{-1}\,atm^{-1}$
Etendu	7.4	7.4	$10^{-2}cm^2$ sr
FOV	8	8	degree
Net transmittance	0.20	0.18	—
Cell thickness	1	1	cm atm.
Detector	HgCdTe	HgCdTe	
D^*	4	4	10^9 cm $Hz^{1/2}/W$
Detection limit (4 K contrast)	70	750	ppm m

temperature of the chopper wheel assembly, including the gas cells and blank sectors, is held at a predetermined value and controlled to better than $\pm$ 0.5 K by means of a pair of thermoelectric coolers with a thermal sensor and electronic control loop.

HgCdTe photoconductive detectors are used and are cooled to 77 K by an open-loop Joule–Thomson nitrogen gas cryogenic system. The system design parameters are summarized in Table I.

B. Signal processing

Due to the nature of the infrared radiative transfer process and the small temperature difference between the radiation source (the ground) and the gas cell, the radiation absorption and emission processes of the gas cell [Eq. (5)] must be accounted for precisely in the signal processing.

The radiance at the detector is composed of incoming radiance passing through the rotating gas cell plus internally generated radiance. To account for the absorption of the incoming radiation by the correlation gas cell, the signals through the reference cell and the correlation cell are balanced [Eq. (4)] by introducing an electronic gain factor on the reference cell signal. The emission from the gas cell (J_c) is compensated for by subtracting a certain percentage of the blank sector signal from the gas cell signal; assuming a thermal equilibrium between the gas and the blank sector. The temperature of the entire chopper wheel, including the gas cells and the blank sector, is maintained at the present value, and in this way the electronic gain factor set in a laboratory remains valid for varying environmental temperatures. Under this condition, and in the absence of the test gas the difference signal ΔS is written, based on Eq. (1), as

$$\Delta S = S_c - g_1 S_r - g_2 S_b, \tag{12}$$

where S_c, S_r, and S_b are the signals from the detector when the correlation gas cell, reference cell, and the blank sector are in the field of view, and g_1 and g_2 are the electrical gain factors. Considering the radiative transfer process,

$$S_c = t_c S_r + (1 - t_c) S_b, \tag{13}$$

where t_c is the gas cell transmittance. Substituting Eq. (13) into Eq. (12) we get

$$\Delta S = t_c S_r + (1 - t_c) S_b - g_1 S_r - g_2 S_b. \tag{14}$$

Since S_r and S_b are independent variables corresponding to the two different temperature Plank functions, respectively, and since the gas singal balance requires these two variables to be insensitive to change, one can write

$$g_1 = t_c, \quad g_2 = 1 - t_c. \tag{15}$$

Under this balance it can be proved that any random noise components are canceled out and the conventional two-phase modulation synchronous detection concept becomes valid. It is important to note that the difference signal is related linearly to the radiance, but with an offset term. The offset term is, in practice, equivalent to a dc component of the noise, and so has no impact on the signal processing algorithm.

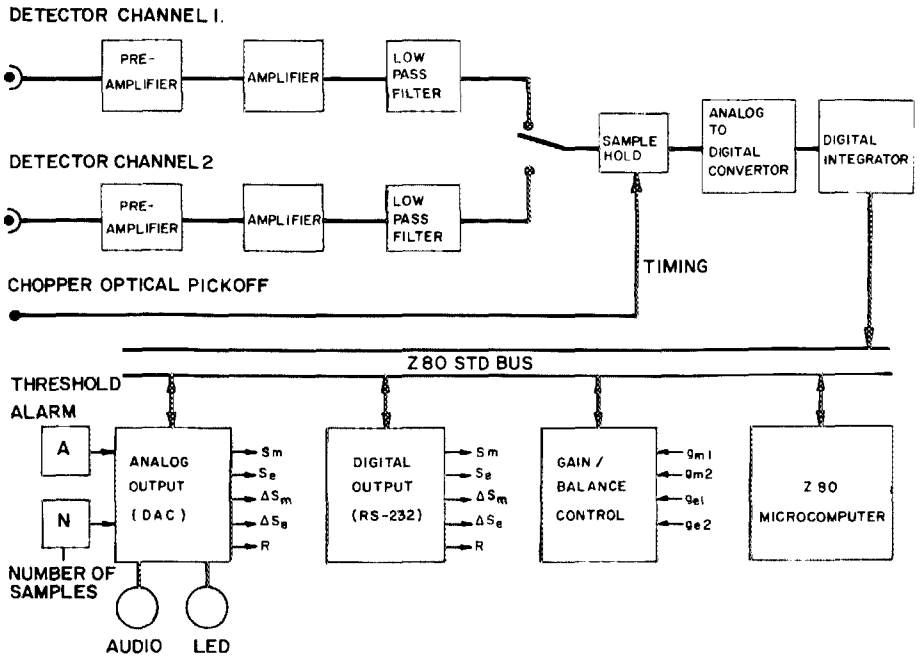

FIG. 4. GASPILS signal processing electronics system.

The signal processing electronics includes the analog amplifiers, filter, digitizer, signal processor, and alarm (leak detector) circuits as shown in Fig. 4. A Z80 microprocessor is used for control and processing. The schematics of the incoming signals from the detector amplifier are shown in Fig. 3. These signals, after the low pass filter, are sampled and digitized 128 times during each sector period, and then averaged. These average values for each sector in each channel are fed to the Z80 microprocessor for "balancing." The gain for the balance condition is selected by means of a pair of 16-bit dip switches. These "balanced" signals are then interpolated to obtain three average values (from two different gas cells and a blank sector) at a common temporal point to compensate for the scene radiance variation. This interpolation, together with the "balancing," comprises a linear filter which reduces the impact of the low-frequency noise component. Note that the signal S_c provides a measure of the scene radiance and (unlike S_r) is largely insensitive to the presence of leak gas.

The values of S and ΔS are then averaged for N selectable samples (one sample per rotation), and the ratio signal is calculated using the averaged results. The signals available at the output of the sensor (in digital and analog form) include $\bar{S}_m$, $\bar{S}_e$, $\Delta\bar{S}_m$, $\Delta\bar{S}_e$ and $R = \Delta\bar{S}_m/\Delta\bar{S}_e$, where subscripts m and e designate the target gases; for example, methane and ethane, respectively. Audio and visual alarms are also provided, which activate when the ratio signal exceeds a preset threshold value.

III. GASPILS PERFORMANCE TEST

A. Laboratory test and sensitivity calibration

The GASPILS sensor performance was first tested in the laboratory. The tests were designed to evaluate its sensitivity to target gas, as well as any false alarm characteristics resulting from , for example, variation in the ground radiance. A variable temperature blackbody source was used to simulate the scene radiance variations, and the test gas optical thickness was varied by injecting known amounts of test gas into a gas cell.

The zero gas "balance" of GASPILS was first set by

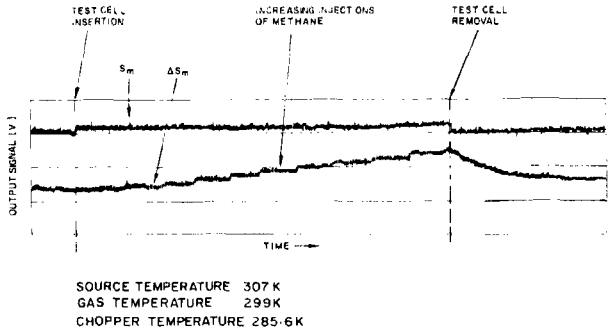

FIG. 6. GASPILS sensitivity calibration data.

varying the temperature of the blackbody source (with no test gas) and adjusting the gain factors for the reference cell sector and the blank sector. Balance was obtained when there were no output variations in the gas signal as the blackbody source temperature was changed by 10 K. Results of balancing are shown in Fig. 5; the balance point remaining unchanged for up to 20 K variation of the source temperature.

Since such large scene changes are not expected,this performance is well within required specifications. The gas detection sensitivity was then measured for both channels. The resulting output signals (gas signal and radiance signal) are shown in Fig. 6, and the gas signal, ΔS is plotted as a function of the test gas optical thickness (ppm m) in Fig. 7. Also shown in this figure is the magnitude of the rms noise level measured during the experiment. Note that the gas signal deviates from the linear behavior as the test gas optical thickness increases; as expected based on the results of the model calculation.

This experiment was repeated for various source temperatures for a fixed test gas temperature, and the detection limit, defined for the signal-to-noise ratio of one, is plotted as a function of the source temperature for a fixed gas temperature in Fig. 8. For a typical summer time field condition (an effective temperature difference of more than 4 K between the source and the target gas[11]), the detection limit for the methane gas, in the field, is estimated from Fig. 8 to be less than 70 ppm m.

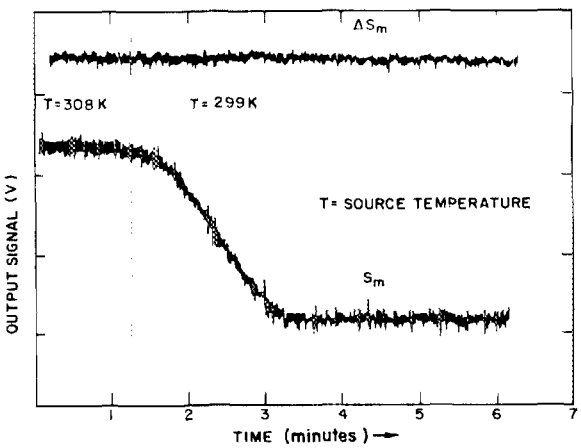

FIG. 5. The zero gas "balance" of GASPILS for a wide range of source temperature.

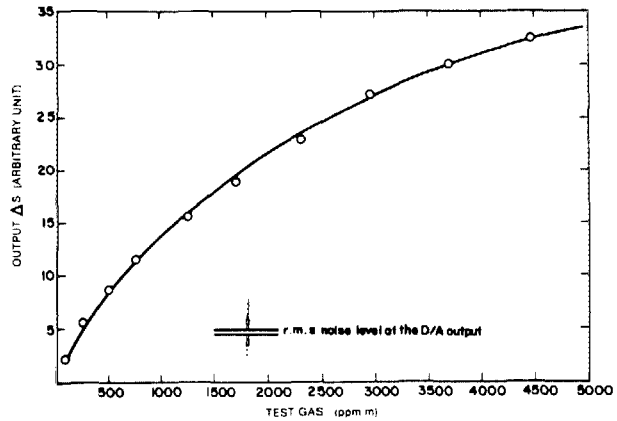

FIG. 7. GASPILS gas detection sensitivity calibration curve at source temperature 308 K and gas (CH_4) temperature 300 K.

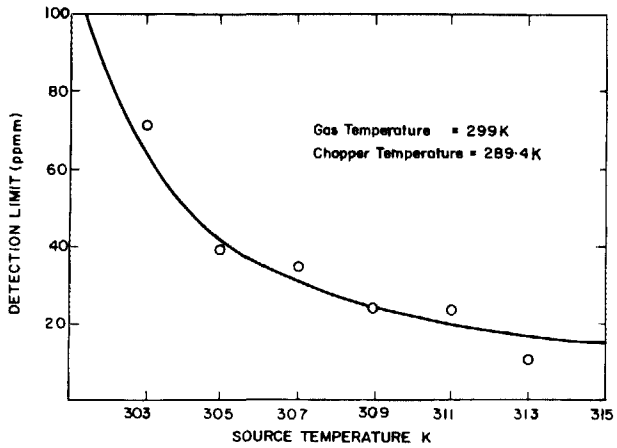

FIG. 8. GASPILS detection limit versus ther mal contrast.

Compared with the methane gas sensitivity and its close agreement with the model calculation prediction, the sensitivity of the ethane channel was considerably lower (750 ppm m for 4 K temperature contrast) than that predicted. This sensitivity was not sufficient to allow the ratio signal to be used to set the gas leak detection threshold. Such a ratio signal would reduce potential problems associated with background methane signal variations and the atmospheric temperature gradients. Since this option would have provided a useful extension of the sensor's capability, new algorithms are being tested as an alternate method of isolating the variations in the ground radiance and the atmospheric temperature gradient. However, such alogrithms are not capable of distinguishing between other sources of natural gas and pipeline gas.

B. Preliminary field test

After these successful laboratory tests, GASPILS was mounted in a helicopter and field tested over a number of different sites. Measurements were made over simulated methane leaks, and ground data (gas concentrations) were collected.

For the maximum sensitivity, one needs to maximize the temperature contrast between the ground and the target gas right above the ground. Existing field data[13] show the maximum contrast between 10 and 15 h during the day reaches as high as 5 K. These data were also confirmed by our own data taken at the vicinity of Addison Airport, Dallas, TX, where the preliminary field test was carried out. It is important to note that the sensor sees a higher average temperature contrast due to the extended temperature gradient throughout the altitude range to the sensor platform altitude ($\sim$100 m). The emissivity of the ground surface at 7.8 μm is fairly constant (0.96) for various ground coverages.[11] Consequently, if the sensor is operated during several hours around noon time, the temperature contrast can be maintained at least 4 K, which was the assumed value in the laboratory test.

The local temperature contrast may change substantially as the sensor footprint moves along the pipeline. This change will directly influence the gas signal due to the residual atmospheric methane gas. In order to distinguish the methane leak signal from the temperature contrast signal, the second channel will be used which will measure another uniformly mixed atmospheric trace gas such as N_2O or other hydrocarbon gases. The ratio of the two gas signals will essentially eliminate the interference from the residual atmospheric methane gas.

Before we implemented further sophisticated concepts, we brought the sensor out to the field to test the methane channel sensivity and to assess unanticipated problems in the field condition. A controlled leak from a natural gas pipeline was set up to simulate relatively small leaks in the middle of an open field. The average ground temperature estimated from the radiance was 15°C and the air temperature at a height of 2 m was measured to be 17° C. The wind speed was 16 km/h. A simultaneous *in situ* measurement was carried out on the ground by means of air sampling and postanalysis of the sample in a chemical laboratory (Geophysical Services, Inc., Dallas, TX) for verification of the GASPILS data. Shown in Fig. 9 is one of the analog output data sets of GASPILS flown over the controlled leak at an altitude of about 30 m. A substantially lower altitude was chosen in this test to minimize the residual atmospheric methane gas effects. The arrows in Fig. 9 indicate the overlap of the sensor footprint with the plume. The gas signal is

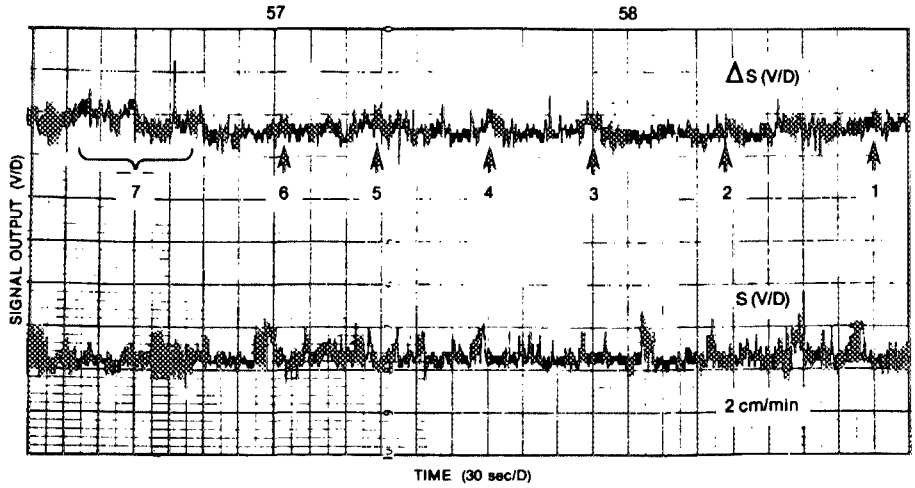

FIG. 9. GASPILS analog signal output as it flies over a controlled pipeline leak at various downwind distances. Arrows indicate the overlap of sensor footprint with the plume. Upper trace, gas signal; bottom trace, radiance signal.

TABLE II. Sample analysis data.

Sample no.	Gas concentration (ppm V)			
	Methane	Ethane	Ethylene	Propane
1001	27.82	1.01	0.06	0.31
1002	11.43	0.33	0.14	0.17
1003	24.00	0.82	0.00	0.24
1004	20.90	0.75	0.00	0.17
1005	7.88	0.07	0.00	0.00
1006	7.59	0.14	0.00	0.00
1007	7.87	0.22	0.15	0.05

clearly distinguishable from the background noise with an average amplitude of three times the rms noise value. It is very important to note that the gas signal and the radiance signal are not strongly correlated due to the low altitude. The high radiance signal does not cause a noticeable gas signal and vice versa.

Table II shows the result of the analysis of the sample taken in the plume along the downwind direction (between 20 and 90 m). Maximum concentration in the sample shows 28 ppm at a 30-m downwind distance from the source. Assuming a plume diameter of 10 m, the total gas overburden is calculated to be 280 ppm m. Since the gas signal amplitude from the GASPILS is about three times the rms nosie value we conclude that the detection limit of the sensor in this field test is about 95 ppm m. Considering the rather low temperature contrast at the time of flight (2°C), the detection sensitivity of the sensor is considered to be in good agreement with the laboratory test results.

In spite of the successful field test on the methane gas detection sensitivity, the sensor still has a major obstacle to overcome. That is the interference from the residual atmospheric methane gas. When the sensor altitude is high (100 m) the cumulative methane below the sensor reaches as high as 160 ppm m. Therefore, fluctuations of the temperature contrast will introduce a false gas signal proportional to the amplitude of the fluctuations. The implementation of the second channel sensitive to the other uniformity mixed atmospheric trace gas and ratioing the two gas signals will help to reduce the problem.

ACKNOWLEDGMENTS

The sensor development program was partly funded by the Department of Supply and Services, Canada, the Department of Energy, Mines, and Resources and by Transport Canada. Partial funding from Recon Exploration in the preliminary field test is also acknowledged. The authors thank Dr. R. A. O'Neil, Canada Centre for Remote Sensing, for helpful discussions and suggestions.

[a] Present address: EG&G WASC, Wallops Island, Virginia 23337.

[1] K. F. Luft, J. Tech. Phys. **24,** 97 (1943).
[2] C. B. Ludwig, R. Bartle, and M. Griggs, NASA CR-1380 (July 1969).
[3] E. R. Bartle, E. A. Meckstroth, and S. Kays, AFRPL TR-71-59 (1971).
[4] A. E. Martin, Research **6,** 172 (1953).
[5] R. Goody, J. Opt. Soc. Am. **58,** 900 (1958).
[6] S. D. Smith and C. R. Pidgeon, in Proceedings of the XIII International Symposium, Liege (June 1963).
[7] T. V. Ward and H. H. Zwick, Appl. Opt. **14,** 2896 (1975).
[8] A. Chedin, N. Huoon, and R. S. McDowell, J. Mol. Spectrosc. **71,** 343 (1978).
[9] R. S. McDowell, J. Mol. Spectrosc. **21,** 280 (1966).
[10] W. R. Rouse, D. Noad,and J. McCutcheon, J. Appl. Meteorol. **12,** 798 (1973).
[11] W. L. Wolfe and G. J. Zissis, *The Infrared Handbook* (ONR, Washington, D.C., 1978).
[12] J. A. Logan, M. J. Prather, S. C. Wofsy, and M. B. McElroy, J. Geophys. Res. **86,** No. C8, 7210 (1981).
[13] *Handbook of Geophysics and Space Environment*, edited by Shea L. Valley (1965), pp. 3–21.